ELECTROMAGNETIC ULF/ELF OSCILLATIONS CAUSED BY THE ERUPTION OF THE TONGA VOLCANO

V.A. Martines-Bedenko ⓘ
Institute of Physics of the Earth RAS,
Moscow, Russia, lera_m0@mail.ru

V.A. Pilipenko ⓘ
Institute of Physics of the Earth RAS,
Moscow, Russia, pilipenko_va@mail.ru

K. Shiokawa ⓘ
Nagoya University,
Nagoya, Japan, shiokawa@isee.nagoya-u.ac.jp

R.R. Akbashev ⓘ
Kamchatka Branch of the Unified Geophysical Survey RAS,
Petropavlovsk-Kamchatsky, Russia, arr@emsd.ru

Abstract. The eruption of the Tonga volcano on January 13 and 15, 2022 and related intense lightning activity led to the excitation of a number of specific electromagnetic oscillations in different frequency ranges. We examine properties of these oscillations, using data from magnetometers of various types located in Kamchatka and in the Pacific region. We confirmed that there might have been a geomagnetic response to the formation of an acoustic resonance between the Earth surface and the ionosphere: localized harmonic oscillations with a frequency 3.5–4.0 mHz, which lasted for ~1.5 hr, were detected ~15 min after the beginning of the eruption at distance of ~800 km. An increase was observed in the intensity of the Schumann resonance at stations in the Far East. Broadband emission stimulated by intense volcanic lightning was detected to occur in the Pc1 range (2–5 Hz). The emission presumably results from the excitation of the magnetosonic waveguide in the upper ionosphere by lightning activity.

Keywords: volcanic eruption, atmospheric waves, acoustic resonance, Schumann resonance, Pc1, ionospheric waveguide.

INTRODUCTION

Volcanic eruptions and earthquakes excite atmospheric acoustic-gravity waves (AGWs) with periods from several minutes to several hours. Modulation of the ionosphere by AGWs allows the planetary detection of the ionospheric response to catastrophic geophysical phenomena with the aid of global navigation satellite systems (GNSS) [Yasyukevich et al., 2013]. When wave disturbances cover a conducting ionospheric layer (~120 km), they cause a response in the geomagnetic field [Kunitsyn, Shalimov, 2011]. Along with these generally observed and well-known effects, geophysical phenomena with a large amount of energy released excite fairly rare specific electromagnetic oscillations.

Among such oscillations are specific Pc5 pulsations, which, unlike magnetospheric Pc5 pulsations, are spatially localized in the vicinity of the epicenter of an earthquake or eruption. These harmonic oscillations can last for several hours, their period significantly exceeding the maximum possible period of the magnetospheric Alfvén resonator in the observation area. For example, 12 min after the 2004 Sumatra earthquake, spatially-localized magnetic Pc5 pulsations with a central frequency of 3.6 mHz were detected at distances up to 1500 km from the epicenter [Iyemori et al., 2005]. Similar periodic pulsations of the ionospheric total electron content (TEC) were also recorded after other strong earthquakes [Choosakul et al., 2009; Saito et al., 2011].

These phenomena were associated with the acoustic resonance between the Earth surface and the ionosphere, which is excited by sharp vertical movements of the Earth surface. The main observed spectral peaks correspond to the periods 260–270, 220–230, and 190–200 s and are presumably linked to the harmonics of acoustic resonator [Tahira, 1995; Nishida et al., 2000], although the period may vary somewhat depending on the state of the atmosphere. According to the numerical simulation results obtained by Shinagawa et al. [2007], the region of barometric variations related to the vertical acoustic resonance is limited to the area above the epicenter, whose size depends on the scale of the earthquake. Nonetheless, the magnetic effect of the acoustic resonance can be observed in a wider area since horizontal ionospheric currents can spread along the conducting ionospheric layer beyond the resonance region. The standing mode of the acoustic resonator in the atmosphere can generate a wave disturbance linked to a propagating seismic Rayleigh wave [Kanamori, Mori, 1992; Kanamori et al., 1994].

A peculiarity of volcanic eruptions as compared to earthquakes is that in addition to the acoustic effect on the atmosphere and ionosphere there is an electromagnetic effect of volcanic lightning. The electrostatic charge in the eruptive cloud is carried by the eruption products: volcanic ash, aerosols, and gases, with up to 98 % of the mass of all gases being water vapor [James et al., 2008; Lane et al., 2011]. Charging of the eruption products is caused by such physical processes as fracto-emission [Behnke et al., 2018; Harper et al., 2021], tribo-electrization [Rulenko et al., 1986; Aplin et al., 2016], and charging during the interaction between the eruptive cloud and hydrometeors [Arason et al.,, 2011; Van Eaton et al., 2020]. During volcanic eruptions in Alaska, three types of lightning discharges occurring at different stages of explosive eruptions have been identified [Thomas et al., 2007]:

I. Crater discharges recorded in the gas pressure region (ash-gas jet injection) at the initial moment of the formation of an eruptive column; their duration is $\sim 10^{-4}$ s, which corresponds to a lightning channel 10−100 m long.

II. Near-crater lightning that features a discharge 0.01–0.1 s long (the length of the lightning channel is 1–7 km). The near-crater lightning arises from further development and rise of the eruptive column, accompanied by an increase in unipolar bulk charges and the scale of charge separation.

III. Classical lightning discharges, similar to those recorded in meteorological clouds, appear when the eruptive column reaches the maximum height. Here, the accumulation of electrostatic charges is driven by the formation of hailstones with ash particles becoming condensation nuclei. The lightning discharge in this case lasts for >0.1 s, which corresponds to a lightning channel >10 km long.

The electromagnetic effect of volcanic lightning can provoke a response in resonant ionospheric systems — the Schumann resonator (SR) and the ionospheric waveguide for MHD waves. SR is a spherical resonator for electromagnetic waves with a fundamental frequency of 7.8 Hz. It is formed by the Earth surface and the lower edge of the ionosphere. SR is generally fed by global thunderstorm activity in tropical regions. The ionospheric MHD waveguide (with a cutoff frequency of ~1 Hz) is formed by dense plasma of the ionospheric F layer. As far as we know, experimental evidence about the excitation of the ionospheric MHD waveguide by lightning discharge has not yet been obtained. The only effect of this kind is the excitation of 2–5 s geomagnetic pulsations by electromagnetic pulse of a high-altitude nuclear explosion, which were detected at a great distance from the explosion site [Fraser, 1962].

TONGA ERUPTION: ATMOSPHERIC, IONOSPHERIC, AND GEOMAGNETIC EFFECTS

A series of explosive eruptions of the underwater volcano Tonga (the full name is Hunga Tonga-Hunga Ha'apai) in the South Pacific Ocean began on January 13, 2022 at 15:20 UT, and the main eruption occurred on January 15, 2022 at 04:15 UT [Yuen et al., 2022]. According to seismic data, this eruption was recorded as an earthquake with magnitude M=5.8 and a focal depth of 0 km. The January 15, 2022 eruption disturbed all geophysical environments, not only in the vicinity of the eruption, but across the globe. The underwater volcanic eruption caused a tsunami that hit the Pacific coast from Japan to the United States. The atmospheric wave excited by the eruption circled the entire globe several times. When analyzing GNSS data, Astafyeva et al. [2022] have found a response of the upper ionosphere to this event — a large increase in TEC followed by a significant long-term decrease. According to the data, the energy released during the explosive eruption was estimated at 9–37 megatons in TNT equivalent.

The ionospheric disturbance might have been caused by a Lamb surface wave propagating with a sound velocity

~300–350 m/s. The greatest disturbance (up to 3 TEC), observed at distances <5000 km, had a velocity of 700 m/s, which gradually decreased to 450 m/s. The ionospheric disturbance came to the west coast of the USA 4 hrs earlier than the tsunami with a characteristic velocity of 210 m/s. The intense atmospheric Lamb wave caused a tsunami precursor, which was several hours ahead of the main wave.

Volcanic lightning during the eruption

A unique feature of the eruption of the underwater volcano Tonga was the strongest volcanic lightning activity. The lightning activity dynamics has been traced using data from the ground-based global lightning detection network GLD360, owned and operated by Vaisala. According to GLD360 data, almost 590000 lightning discharges occurred for three days of the eruption. When the first eruption began on January 13 at 15:20 UT, the surrounding islands of the Tonga Archipelago were completely engulfed by lightning. Lightning activity continued with varying intensity for several days. An even more powerful underwater eruption on January 15 caused the most intense burst of lightning activity with almost 400000 discharges recorded for 6 hrs. At the peak of activity, 200000 discharges per hour were detected, which accounted for 80 % of hourly average thunderstorm activity worldwide. During the eruption on Tonga, lightning was observed both during the dry charging phase on January 13 when the eruption plume was below 55 km, and during the ice charging phase on January 15 when the eruptive cloud reached a height of 55 km.

Magnetic effects

The eruption on January 15 occurred during the recovery phase of a moderate magnetic storm with $|Dst| \sim 94$ nT, which began on January 14 at 23 UT when the geomagnetic field was still slightly disturbed. The ICON and Swarm satellites observed the effect of the atmospheric disturbance over Central America on the dynamo region of the ionosphere [Harding et al., 2022]. After the Lamb wave reached the dayside, Swarm A detected an intense equatorial electrojet in two consecutive orbits; and ICON recorded extreme neutral wind speeds at 90–300 km. Harding et al. [2022] have assumed that the electrojet disturbance was caused by a strong wind in the dynamo layer of the ionosphere (~120–150 km).

Acoustic resonance excitation during eruptions and earthquakes has been found from geomagnetic data in [Iyemori et al., 2022; Yamazaki et al., 2022].

The following geomagnetic effects of the strong disturbances generated by the powerful eruption on January 15 might also have been expected.

• Geomagnetic variations induced by the movement of the tsunami. These effects can be identified at the island observatories through which the tsunami passed [Sorokin et al., 2019].

• An atmospheric wave propagating along the ionosphere and covering the conductive E layer of the ionosphere could excite geomagnetic disturbances at ground

stations [Pogoreltsev, 1989]. The time delay between the stations should correspond to the velocity of atmospheric wave propagation.

In this paper, we demonstrate the effects of excitation of the acoustic Pc5 resonance, SR, and MHD waveguide during the Tonga volcano eruption, using data from magnetometers in the Pacific and Far Eastern regions.

OBSERVATIONS OF ULF PULSATIONS INDUCED BY THE ERUPTION

We have analyzed data from INTERMAGNET magnetometers with a sampling period of 1 min (see the location of the selected stations in the Pacific region in Figure 1). These three-component fluxgate magnetometers have a flat frequency response.

At the API magnetic station closest to the Tonga Archipelago (at $R{\sim}800$ km), quasi-monochromatic oscillations with two bursts from 04:30 to 05:50 UT were recorded ~15 min after the eruption (Figure 2). The oscillations are most pronounced in the Y component of the geomagnetic field (with the highest amplitude of ~6 nT) and are much weaker in the Z (~4 nT) and X (~2 nT) components. At the stations more remote from the eruption site ($R{>}2500$ km) and at higher latitudes, these oscillations no longer manifest themselves.

Oscillation frequencies have been estimated through spectral analysis (Figure 3). Harmonics with frequencies of 3.5 mHz (4.8 min period) and 4.0 mHz (4.2 min period) are clearly seen in the spectrum. According to all morphological features, these Pc5 pulsations are not ordinary magnetospheric oscillations, but are caused by the acoustic resonance.
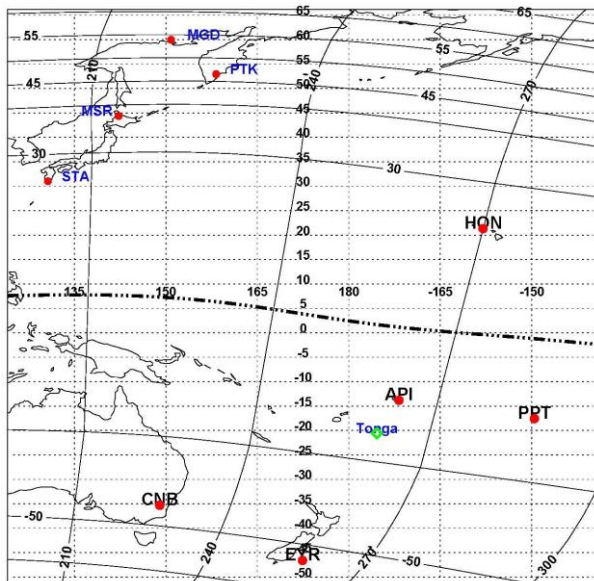

Figure 1. Map of magnetic stations equipped with fluxgate (red dots) and induction (blue font) magnetometers. The green rhombus marks the epicenter of the volcanic eruption; solid lines, the geomagnetic coordinate grid; the dash-dot line is the geomagnetic equator
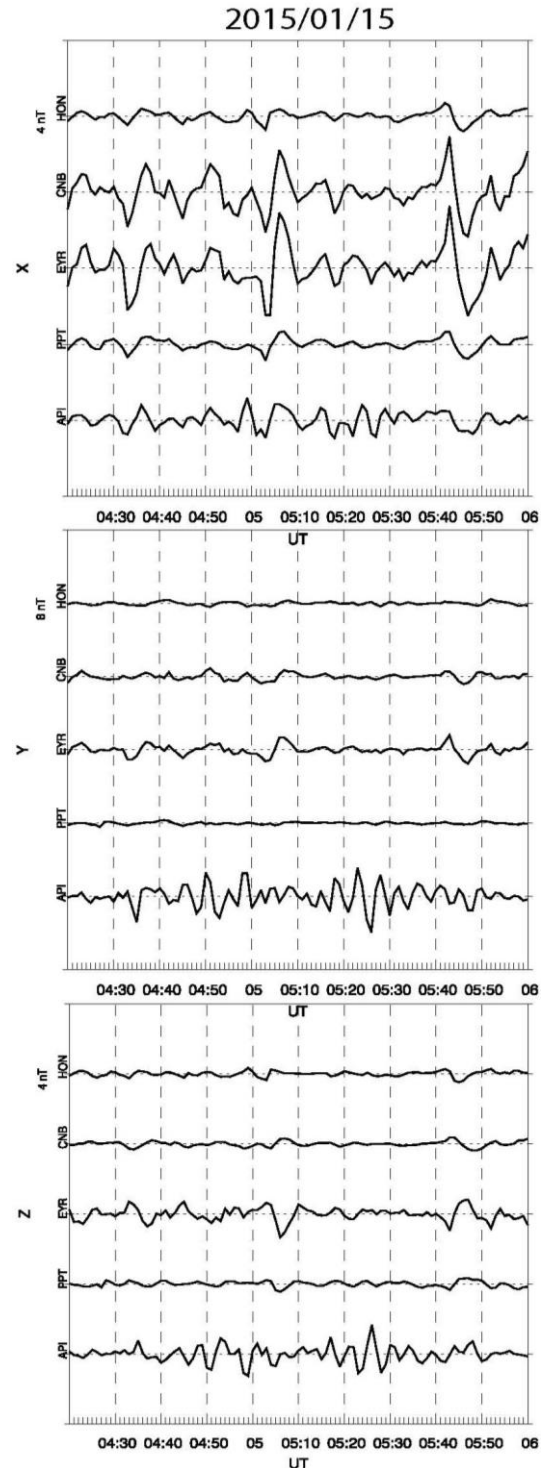

2015/01/15

Figure 2. Magnetograms of the X, Y, Z components at the HON, CNB, EYR, PPT, API stations at 04:20–06:00 UT, January 15, 2022

Phase relations between the pulsation field components can be qualitatively estimated from filtered 1 sec magnetograms (2 mHz cutoff frequency) from the API and HON stations (Figure 4). The second burst of oscillations is most pronounced. It is observed not only in the Southern Hemisphere at API, but also in the Northern Hemisphere at HON. At the same time, at other stations in the Southern Hemisphere, the Pc5 pulsations of interest cannot be distinguished even after filtration. At the API station nearest
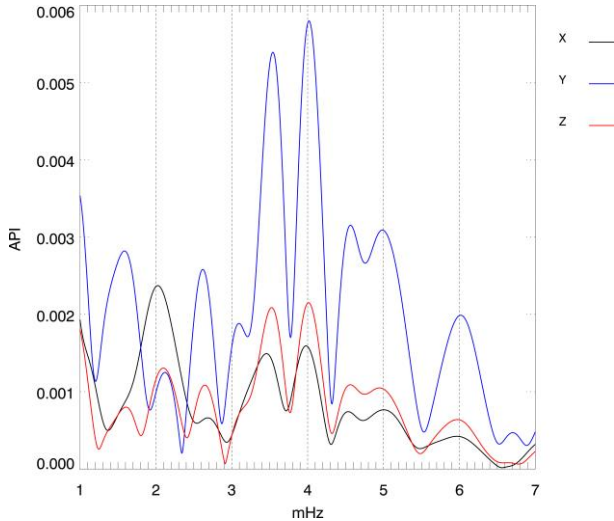
Figure 3. Spectrum of magnetic variations in the X ,Y, Z component at the API station at 04:30–05:50 UT, January 15, 2022
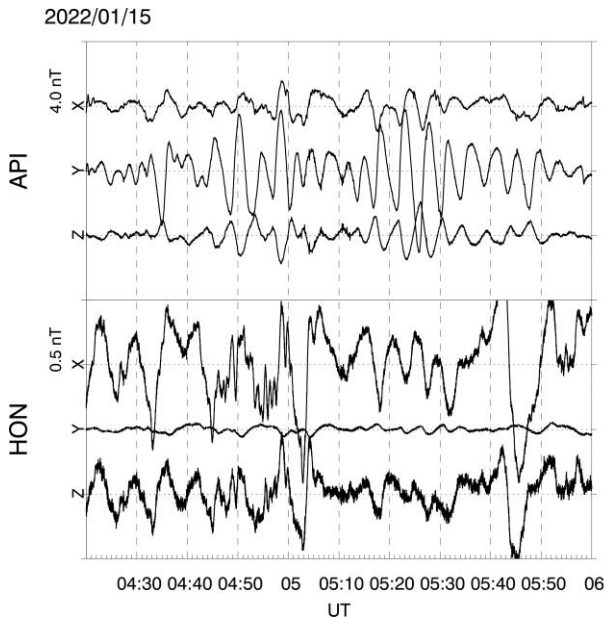

Figure 4. Geomagnetic response to the acoustic resonance (X, Y, Z components) at the API and HON stations at 04:20–06:00 UT, January 15, 2022 (pre-filtration with a cutoff frequency of 2 mHz). Along the Y axis is the vertical scale of the magnetograms — the distance between marks is in nT

to the epicenter of the eruption, the Y- and Z-component pulsations are in antiphase. The X-component pulsations turn out to be in-phase in the Southern (API) and Northern (HON) hemispheres. The appearance of a response in the other hemisphere may indicate that part of the energy of the geomagnetic disturbance is transferred by field-aligned currents to the conjugate region of the ionosphere.

OBSERVATIONS OF SR AND Pc1 PULSATIONS, EXCITED BY VOLCANIC THUNDERSTORMS

Data for the analysis includes records of ULF/ELF variations in Earth's electromagnetic field made at a network of stations of the PWING project (Study of

Dynamic Variation of Particles and Waves in the Inner Magnetosphere Using Ground-Based Network Observations) [Shiokawa et al., 2010] equipped with 64 Hz induction magnetometers. This network of stations has been deployed as ground support for the ERG (Arase) satellite project. Location of the stations is shown in Figure 1; their geographical coordinates and distances to the epicenter of the eruption are listed in Table. The vertical component (Z) in the magnetometer data is noisy and therefore omitted from the analysis. We analyze only the horizontal north–south (X) and east–west (Y) components. The amplitude-frequency response of the induction magnetometers increases linearly with frequency, having a wide maximum at 1.5–5.0 Hz, and decreases at >5 Hz. This equipment can record Pc1 pulsations (from 0.1 Hz to several Hz) and SR emission, even if in a weakened form due to peaculiarities of the frequency response.

Coordinates of magnetic stations and distance to the eruption site

Code	Name	Latitude	Longitude	R, km
	Tonga	–20.55	–175.39	
Fluxgate magnetometers				
API	Apia	–13.80	–171.78	813
PPT	Pamatai	–17.57	–149.58	2710
EYR	Eyrewell	–46.60	172.40	2552
CNB	Canberra	–35.30	149.00	3797
HON	Honolulu	21.32	–158.00	5094
IPM	Easter Island	–27.20	–109.42	6656
Induction magnetometers				
MSR	Moshiri	44.37	142.27	8437
MGD	Magadan	59.97	150.86	9508
STA	Sata	46.09	144.19	8476
PTK	Paratunka	52.94	158.25	8548

In the data from PWING induction magnetometers, SR is manifested only at the MSR and STA stations because frequencies above several Hz are suppressed by the frequency response. At these stations, the spectral amplitude at the SR frequency experiences a maximum increase at ~05 UT, which coincides in time with the highest volcanic lightning activity (Figure 5). This increase results from an increase in the density of atmospherics and their intensity [Nickolaenko et al., 2022].

During the highest lightning activity in the Pc1 range, a broadband burst also appears on the sonograms in the 2–5 Hz frequency band at MSR, PTK, and MGD. At the ZGN station most distant from the eruption site, this burst no longer appears, although this station is located at higher latitudes; and Pc1 pulsations, if they were of magnetospheric origin, should be more pronounced at it. Pc1 pulsations were observed at STA, MSR during the first burst of volcanic lightning activity on January 13 from 16 to 17 UT (Figure 6). The Pc1 pulsations were even more clearly manifested during the most powerful burst of volcanic lightning on January 15 (Figure 7). Pc1 oscillations appeared after the eruption and ended when volcanic lightning activity began to decrease.
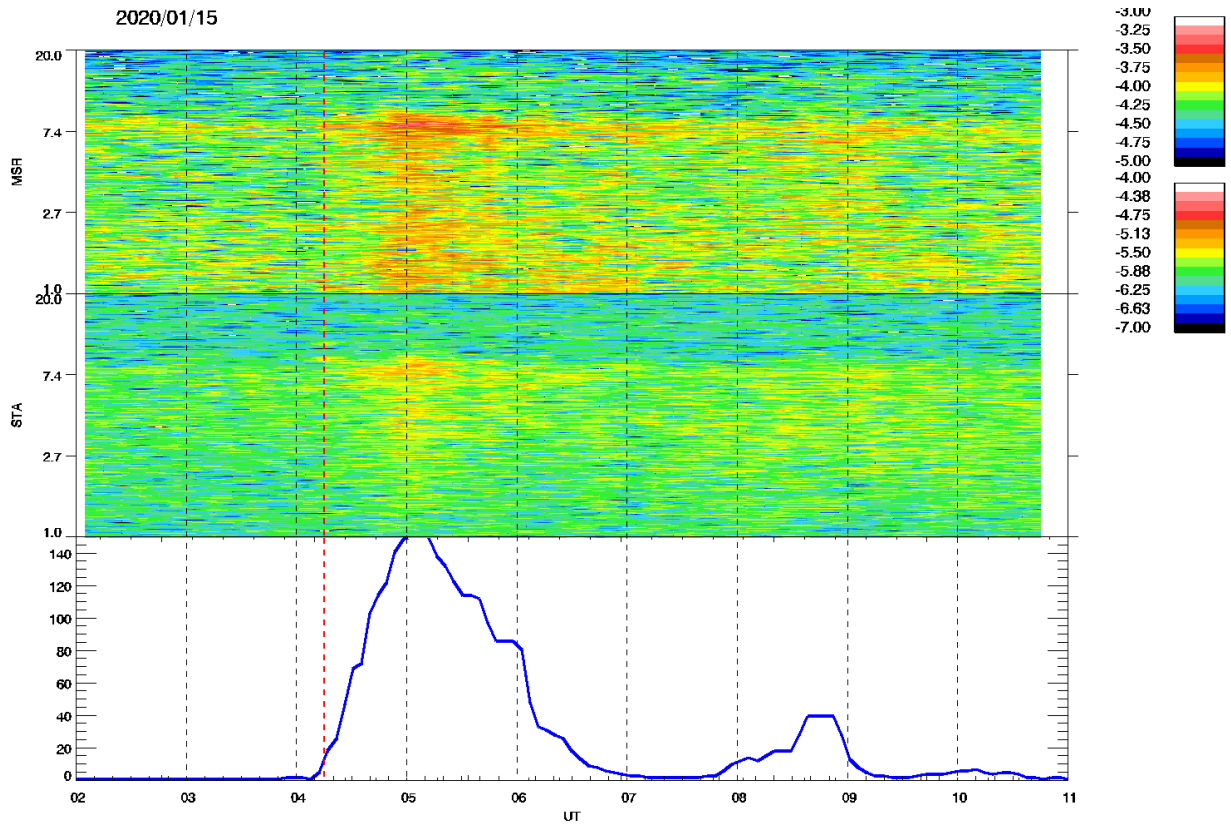
Figure 5. In the top panel are sonograms (1–20 Hz, logarithmic frequency scale) of the Schumann resonance (Y component) from the MSR and STA stations for 02–11 UT, January 15, 2022. In the bottom panel is the volcanic lightning intensity (number of discharges per minute)
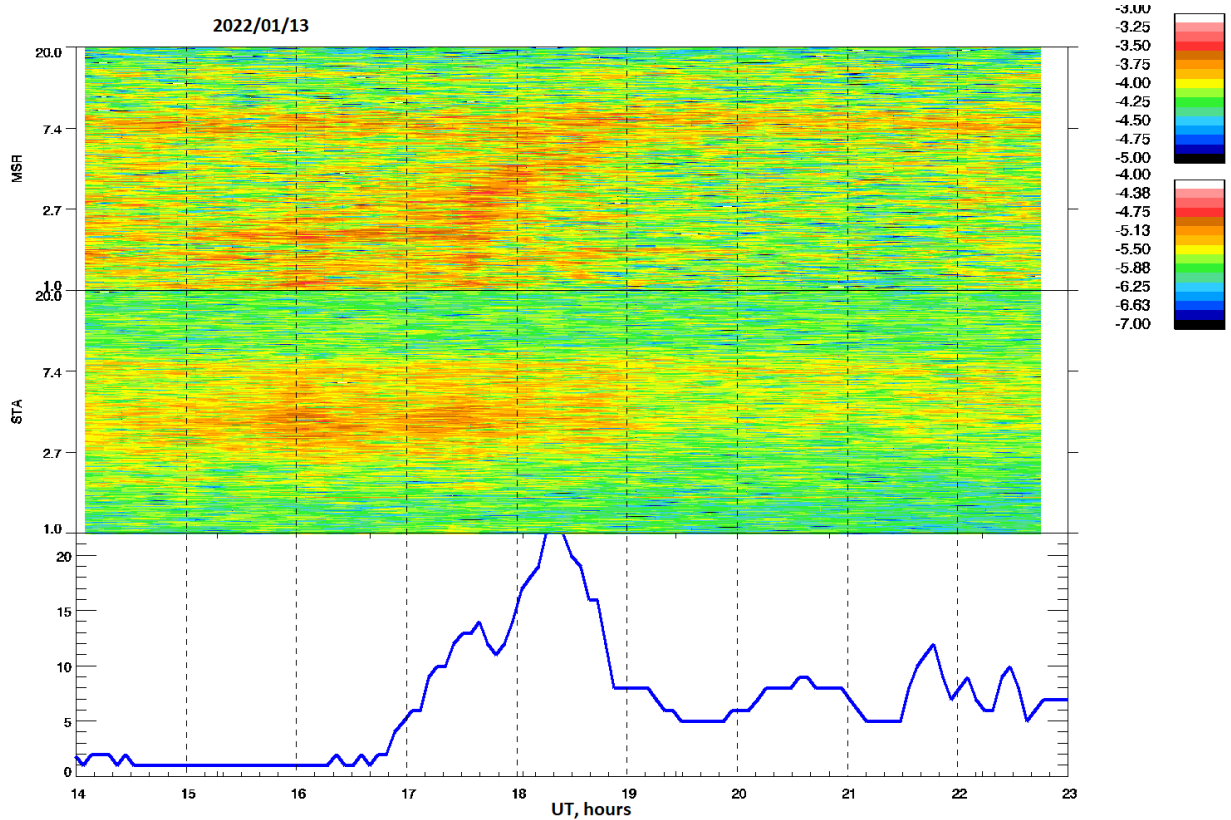

Figure 6. The top panel contains sonograms (1–20 Hz, logarithmic frequency scale) of Pc1 oscillations (Y component) at the MSR and STA stations for 14–23 UT, January 13, 2022. In the bottom panel is the volcanic lightning intensity (number of discharges per minute)
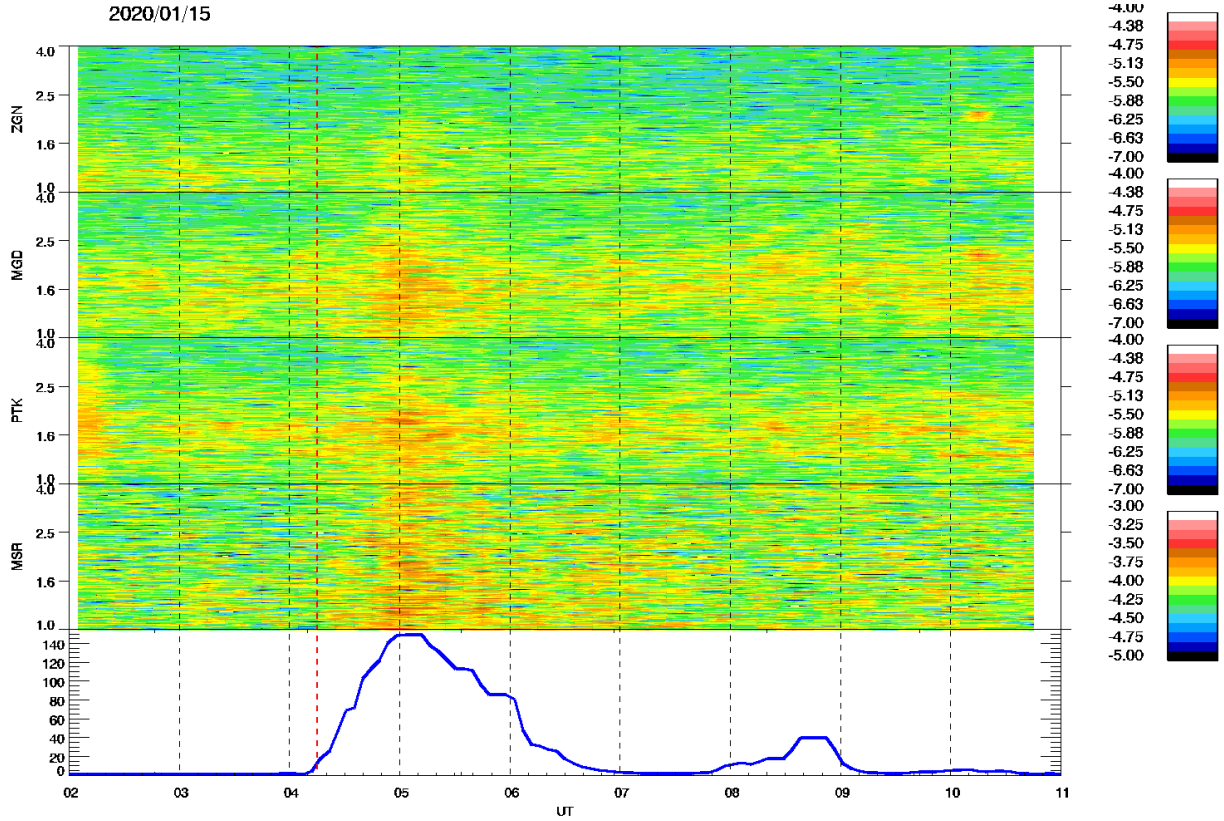
Figure 7. Sonograms of Pc1 oscillations (0.1–4.0 Hz, Y component) at ZGN, MGD, PTK, and MSR for 02–11 UT, January 15, 2022. In the bottom panel is the volcanic lightning intensity (number of discharges per minute)

A characteristic feature of the upper ionosphere is the presence of an ionospheric Alfvén resonator (IAR) and a waveguide for fast magnetosonic (FMS) waves, which can accumulate electromagnetic wave energy in the range from fractions of Hz to several Hz. Numerical simulation of the excitation of electromagnetic modes of IAR and FMS waveguide has been carried out in [Fedorov et al., 2016; Mazur et al., 2018]. The model is based on the numerical solution of coupled wave equations for MHD modes in ionospheric plasma. The vertical profile of ionospheric parameters is reconstructed using an empirical ionosphere model, IRI. Simulation shows that during a lightning discharge (vertical dipole) a coupled wave system consisting of IAR and MHD-waveguide modes is excited. We have used the model developed in [Fedorov et al., 2016; Mazur et al., 2018] to calculate the spectral composition of ULF electromagnetic emission at different distances from the surface source (Figure 8). Near lightning (at distances up to several hundred kilometers), only the lowest IAR harmonics are manifested in spectra of the magnetic component. At large distances (>800 km), the spectral structure is formed mainly by the harmonics of ionospheric waveguide. The waveguide modes are likely to cause the broadband burst in the Pc1 frequency range at stations in Japan and Kamchatka during volcanic lightning activity.

DISCUSSION

According to all morphological characteristics, the Pc5 pulsations, which began at API on January 15 ~15 min
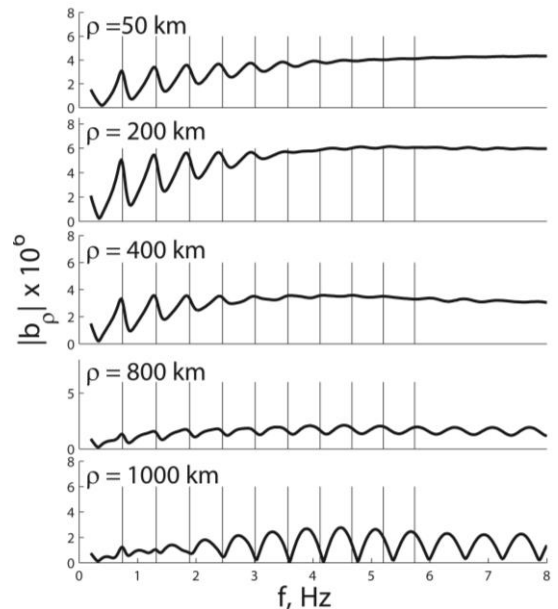

Figure 8. Numerical simulation of excitation of ionospheric electromagnetic modes by a thunderstorm discharge with the model [Fedorov et al., 2016; Mazur et al., 2018]: spectral amplitude of the magnetic component at different distances ρ from the source — a vertical dipole. Vertical lines indicate local resonant frequencies of IAR

after the start of the explosive eruption, were driven by an acoustic resonance. The resonance can qualitatively be represented as acoustic oscillations in a tube closed on one side and open on the other. In an inhomogeneous medium,

acoustic oscillations can propagate only in the region where their frequency f is higher than the critical frequency $f_a = \gamma g / 2\pi V_s$, where $V_s = \sqrt{\gamma P / \rho}$ is the sound velocity. In the real atmosphere, the vertical profile $f_a(z)$ has the main maximum at $z \sim 100$ km and an additional one at $z \sim 30$ km [Matsumura et al., 2009]. At z^*, where $f = f_a(z^*)$, an upward propagating ($\sim \exp(ik_z z)$) acoustic wave is reflected, thereby giving rise to a standing wave whose frequency is determined by the quantization condition $\int_0^{z^*} k_z dz = \pi n / 2$.

Acoustic waves with $f > 5$ mHz freely penetrate into the upper ionosphere, and waves with $f < 3$ mHz are reflected at 20–30 km; and only at intermediate frequencies 3–5 mHz, an acoustic resonance is formed between the Earth surface and the ionosphere with a reflection point at ~ 100 km. The frequency in each event is determined by the vertical profile of atmospheric temperature and density. The standing acoustic wave covers conducting layers of the ionosphere, and the dynamo effect can lead to excitation of current and magnetic field oscillations in these layers [Zettergren, Snively, 2015]. However, as far as we know, the geomagnetic response and field-aligned currents excited by acoustic resonance have not yet been simulated.

The first ionospheric response to the Tonga volcano eruption was detected in its immediate vicinity (~ 200 km), where the apparent propagation velocity of the disturbance, ~ 1050 m/s, was almost three times the speed of sound [Zhang et al., 2022]. According to Themens et al. [2022], such supersonic velocities might have resulted from the formation of a strong shock wave. We believe that these disturbances traveling at supersonic speed were caused by a slow MHD wave propagating in collisional ionospheric plasma. A low-frequency disturbance with a frequency much lower than the frequency of neutral-ion collisions, $\omega \ll \upsilon_{ni}$, will involve neutral particles of the ionosphere in wave motion [Sorokin, Fedorovich, 1982; Nekrasov, Pilipenko, 2020]. As a result, MHD waves will be "loaded" not only with plasma ions, but also with neutral particles, which will lead to a sharp decrease in the propagation velocity. Thus, a slow FMS wave will propagate not with the usual Alfvén velocity V_A, but with a modified Alfvén velocity

$$\tilde{V}_A = V_A \sqrt{N_i / (N_n + N_i)},$$

which is estimated to be of the order of a few kilometers per second in the ionosphere.

We did not manage to detect geomagnetic disturbances caused by atmospheric waves or tsunamis in the available data. We failed in our attempt to find disturbances corresponding to either a sound velocity of ~ 320 m/s or a tsunami wave velocity of ~ 200 m/s, for which there is a difference in arrival times at magnetic stations located at different distances from the source. To confidently single out such effects, it is necessary to analyze magnetometer data together with the data from nearby barometers or buoy mareographs (such as DART). To date, we do not have such data yet.

Extremely high electrical activity at the moment of the Tonga volcano eruption, concentrated in an eruptive cloud, led to a widespread increase in the intensity of electromagnetic noise throughout the SR frequency range, as recorded by induction magnetometers in Italy, France, and Russia; it lasted until the end of the eruption [Nickolaenko et al., 2022]. Our observations at stations in Japan and Kamchatka confirm this finding.

A characteristic feature of the upper ionosphere is the presence of an ionospheric Alfvén resonator and a waveguide for fast magnetosonic waves, which can accumulate electromagnetic wave energy in the range from fractions of Hz to several Hz. Numerical simulation shows that during a thunderstorm discharge (vertical dipole) near lightning (several hundred kilometers), only the lowest harmonics of IAR are manifested in electromagnetic response spectra; and at large distances (>800 km), the spectral structure is formed mainly by the harmonics of FMS waveguide modes. Thus, the simulation predicts that the ionospheric waveguide modes will be observed at a great distance from vertical lightning discharges from ~ 1 Hz to almost the SR frequencies. The predicted pattern is qualitatively consistent with the observations of Pc1 pulsations in Kamchatka and Japan.

CONCLUSION

Observations at magnetic stations in the Pacific and Far Eastern regions have confirmed the possibility of excitation of specific electromagnetic oscillations induced by the explosive volcanic eruption and volcanic lightning activity. At a distance of ~ 800 km from the epicenter of the eruption, local geomagnetic Pc5 pulsations were recorded which, according to morphological characteristics, were triggered by the acoustic resonance between the Earth surface and the ionosphere. An increase in the intensity of the fundamental harmonic of the Schumann resonance during the development of lightning in the eruptive cloud has been confirmed. We have found that the broadband (2–5 Hz) emission in the Pc1 range was excited by volcanic lightning at a considerable distance from the epicenter of the eruption. Numerical simulation has shown that this emission might have been caused by the excitation of the magnetosonic waveguide in the upper ionosphere by lightning activity.

REFERENCES

Aplin K.L., Bennett A.J., Harrison R.G., Houghton I.M.P. Electrostatics and in situ sampling of volcanic plumes. *Volcanic Ash: Hazard Observation and Monitoring*. Amsterdam: Elsevier, 2016, pp. 99–113. DOI: 10.1016/B978-0-08-100405-0.00010-0.

Arason P., Bennett A.J., Burgin L.E. Charge mechanism of volcanic lightning revealed during the 2010 eruption of Eyjafjallajökull. *J. Geophys. Res.* 2011, vol. 116, B00C03. DOI: 10.1029/2011JB008651.

Astafyeva E., Maletckii B., Mikesell T.D., Munaibari E., Ravanelli M., Coisson P., et al. The 15 January 2022 Hunga Tonga eruption history as inferred from ionospheric observations. *Geophys. Res. Lett.* 2022, vol. 49, e2022GL098827. DOI: 10.1029/2022GL098827.

Behnke S., Edens H., Thomas R., Smith C., Mcnutt S., Van Eaton A., Cigala V. Investigating the origin of continual radio frequency impulses during explosive volcanic eruptions. *J. Geophys. Res.: Atmos.* 2018, vol. 123, iss. 8, pp. 4157–4174. DOI: 10.1002/2017JD027990.

Choosakul N., Saito A., Iyemori T., Hashizume M. Excitation of 4-min periodic ionospheric variations following the great Sumatra-Andaman earthquake in 2004. *J. Geophys. Res.* 2009, vol. 114, A10313. DOI: 10.1029/2008JA013915.

Fedorov E., Mazur N., Pilipenko V., Baddeley L. Modeling the high-latitude ground response to the excitation of the ionospheric MHD modes by atmospheric electric discharge. *J. Geophys. Res.* 2016, vol. 121, pp. 11282–11301. DOI: 10.1002/2016JA023354.

Fraser B.J. Geomagnetic micropulsations from the high altitude nuclear explosion above Johnston Island. *J. Geophys. Res.* 1962, vol. 67, p. 4926.

Harding B.J., Wu Y.-J.J., Alken P., Yamazaki Y., Triplett C.C., Immel T.J., et al. Impacts of the January 2022 Tonga volcanic eruption on the ionospheric dynamo: ICON-MIGHTI and Swarm observations of extreme neutral winds and currents. *Geophys. Res. Lett.* 2022, vol. 49, e2022GL098577. DOI: 10.1029/2022GL098577.

Harper M.J., Cimarelli C., Cigala V., Kueppers U., Dufek J. Charge injection into the atmosphere by explosive volcanic eruptions through triboelectrication and fragmentation charging. *Earth and Planetary Sci. Lett.* 2021, vol. 574, 117162. DOI: 10.1016/j.epsl.2021.117162.

Iyemori T., Nose M., Han D.-S., Gao Y., Hashizume M., Choosakul N., Shinagawa H., et al. Geomagnetic pulsations caused by the Sumatra earthquake on December 26, 2004. *Geophys. Res. Lett.* 2005, vol. 32, L20807. DOI: 10.1029/2005GL024083.

Iyemori T., Nishioka M., Otsuka Y., Shinbori A. A confirmation of vertical acoustic resonance and field-aligned current generation just after the 2022 Hunga Tonga Hunga Ha'apai volcanic eruption. *Earth, Planets and Space.* 2022, vol. 74, 103. DOI: 10.1186/s40623-022-01653-y.

James M.R., Wilson L., Lane S.J., Gilbert J.S., Mather T.A., Harrison R.G., Martin R.S. Electrical charging of volcanic plumes. *Planetary Atmospheric Electricity.* NY, Springer, 2008, pp. 399–418.

Kanamori H., Mori J. Harmonic excitation of mantle Rayleigh waves by the 1991 eruption of Mount Pinatubo, Philippines. *Geophys. Res. Lett.* 1992, vol. 19, pp. 721–724. DOI: 10.1029/92GL00258.

Kanamori H., Mori J., Harkrider D.G. Excitation of atmospheric oscillations by volcanic eruptions. *J. Geophys. Res.* 1994, vol. 99, pp. 21947–21961.

Kunitsyn V.E., Shalimov S.L. Ultralow-frequency variations of the magnetic field during the propagation of acoustic-gravity waves in the ionosphere. *Herald of Moscow University. Ser. 3. Phys. Astron.* 2011, no. 5, p. 75. (In Russian).

Lane S.J., James M.R., Gilbert J.S. Electrostatic phenomena in volcanic eruptions. *J. Phys.: Conf. Ser.* 2011, vol. 301, 012004, pp. 1–4. DOI: 10.1088/1742-6596/301/1/012004.

Matsumura M., Iyemori T., Tanaka Y., Han D., Nose M., Utsugi M., Oshiman N., et al. Acoustic resonance between ground and thermosphere. *Data Sci. J.* 2009, vol. 8, pp. 68–77.

Mazur N.G., Fedorov E.N., Pilipenko V.A., Vakhnina V.V. ULF electromagnetic field in the upper ionosphere excited by lightning. *J. Geophys. Res.* 2018, vol. 123, pp. 6692–6702. DOI: 10.1029/2018JA025622.

Nekrasov A.K., Pilipenko V.A. MHD waves in the collisional plasma of the solar corona and terrestrial ionosphere. *Solar-Terr. Phys.* 2020, vol. 6, no. 4, pp. 17–23. DOI: 10.12737/stp-64202003.

Nickolaenko A.P., Schekotov A.Y., Hayakawa M., Romero R., Izutsu J. Electromagnetic manifestations of Tonga eruption in Schumann resonance band. *J. Atmos. Solar-Terr. Phys.* 2022, vol. 237, 105897. DOI: 10.1016/j.jastp.2022.105897.

Nishida K., Kobayashi N., Fukao Y. Resonant oscillations between the solid Earth and the atmosphere. *Science.* 2000, vol. 287, pp. 2244–2246.

Pogoreltsev A.I. Disturbances of electric and magnetic fields caused by the interaction of atmospheric waves with ionospheric plasma, *Geomagnetism Aeronomy.* 1989, vol. 29, no.2, pp. 286–292. (In Russian).

Rulenko O.P., Klimin N.N., Dyakonova I.I., Kiriyanov V.Yu. Studies of the electrization of clouds created by the dispersion of volcanic ash. *Volcanology and seismology.* 1986, no. 5, pp. 17–29. (In Russian).

Saito A., Tsugawa T., Otsuka Y., Nishioka M., Iyemori T., Matsumura M., Saito S., et al. Acoustic resonance and plasma depletion detected by GPS total electron content observation after the 2011 off the Pacific coast of Tohoku Earthquake. *Earth Planets Space.* 2011, vol. 63, pp. 863–867.

Shinagawa H., Iyemori T., Saito S., Maruyama T. A numerical simulation of ionospheric and atmospheric variations associated with the Sumatora earthquake on December 26, 2004. *Earth Planets Space.* 2007, vol. 59, pp. 1015–1026.

Shiokawa K., Nomura R., Sakaguchi K., Otsuka Y., Hamaguchi Y., Satoh M., Katoh Y., et al. The STEL induction magnetometer network for observation of high-frequency geomagnetic pulsations. *Earth Planets Space.* 2010, vol. 62, pp. 517–524.

Sorokin V.M., Fedorovich G.V. *Fisika medlennykh MGD-voln v ionosfernoi plazme* [Physics of Slow MHD Waves in Ionospheric Plasma]. Moscow, Energoizdat, 1982, 135 p. (In Russian).

Sorokin V.M., Yashchenko A.K., Surkov V.V. Generation of geomagnetic disturbances in the ionosphere by a tsunami wave. *Geomagnetism and Aeronomy.* 2019, vol. 59, no. 2, pp. 221–233. DOI: 10.1134/S0016793219020130.

Tahira M. Acoustic resonance of the atmosphere at 3.7 mHz. *J. Atmos. Sci.* 1995, vol. 52, pp. 2670–2674.

Themens D.R., Watson C., Žagar N., Vasylkevych S., Elvidge S., McCaffrey A., Prikryl P., et al. Global propagation of ionospheric disturbances associated with the 2022 Tonga volcanic eruption, *Earth and Space Science Open Archive,* 2022. DOI: 10.1002/essoar. 10510350.1.

Thomas R.J., Krehbiel P., Rison W., Edens H., Aulich G., Winn W.P., Mcnutt S.R., Tytgat G., Clark E. Lightning and electrical activity during the 2006 eruption of Augustine volcano. *The 2006 eruption of Augustine volcano*, *Alaska.* Professional Paper 1769. U.S. Department of the Interior; U.S. Geological Survey, 2007, pp. 579–608.

Van Eaton A.R., Schneider D.J., Smith C.M., Haney M.M., Lyons J.J., Said R., Fee D., Holzworth R.H., Mastin L.G. Did ice-charging generate volcanic lightning during the 2016–2017 eruption of Bogoslof volcano, Alaska? *Bulletin of Volcanology.* 2020, vol. 82. DOI: 10.1007/s00445-019-1350-5.

Yamazaki Y., Soares G., Matzka J. Geomagnetic detection of the atmospheric acoustic resonance at 3.8 mHz during the Hunga Tonga eruption event on 15 January 2022. *J. Geophys. Res.* 2022, vol. 127, e2022JA030540. DOI: 10.1029/2022JA030540.

Yasyukevich Yu.V., Edemsky I.K., Perevalova N.P., Polyakova A.S. *Otklik ionosfery na gelio- i geofizicheskie vozmushchayushchie faktory po dannym GPS* [Response of the ionosphere to helio- and geophysical disturbing factors ac-

cording to GPS data]. Irkutsk, Irkutsk State University Publ., 2013, 259 p. (In Russian).

Yuen D.A., Scruggs M.A., Spera F.J., Zheng Y., Hu H., McNutt S.R., Thompson G., et al. Under the surface: Pressure-induced planetary-scale waves, volcanic lightning, and gaseous clouds caused by the submarine eruption of Hunga Tonga-Hunga Ha'apai volcano. *Earthquake Research Advances.* 2022, vol. 2, iss. 3, 100134. DOI: 10.1016/j.eqrea.2022.100134.

Zettergren M.D., Snively J.B. Ionospheric response to infrasonic-acoustic waves generated by natural hazard events. *J. Geophys. Res.* 2015, vol. 120, pp. 8002–8024. DOI: 10.1002/2015JA0211-16.

Zhang S-R., Vierinen J., Aa E., Goncharenko L.P., Erickson P.J., Rideout W., Coster A.J., Spicher A. 2022 Tonga volcanic eruption induced global propagation of ionospheric disturbances via Lamb waves. *Front. Astron. Space Sci.* 2022, vol. 9, 871275. DOI: 10.3389/fspas.2022.871275.

URL: www.intermagnet.org (accessed September 29, 2022).

URL: https://graphics.reuters.com/TONGA-VOLCANO/LIGHTNING/zgpomjdbypd/ (accessed September 29, 2022).

How to cite this article
Martines-Bedenko V.A., Pilipenko V.A., Shiokawa K., Akbashev R.R. Electromagnetic ULF/ELF oscillations caused by the eruption of the Tonga volcano. *Solar-Terrestrial Physics*. 2023. Vol. 9. Iss. 1. P. 47–55. DOI: 10.12737/stp-91202306.